Geological modelling from field data and geological knowledge, Part I – Modelling method coupling 3D potential-field interpolation and geological rules

Philippe Calcagno, Jean-Paul Chilès, Gabriel Courrioux, A. Guillen

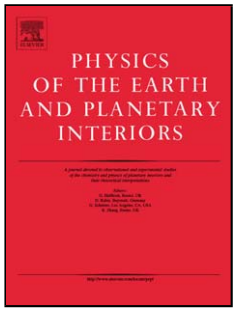

Title: Geological modelling from field data and geological knowledge, Part I – Modelling method coupling 3D potential-field interpolation and geological rules

Authors: P. Calcagno, J.P. Chilès, G. Courrioux, A. Guillen

PII: S0031-9201(08)00125-8
DOI: doi:10.1016/j.pepi.2008.06.013
Reference: PEPI 4968

To appear in: *Physics of the Earth and Planetary Interiors*

Received date: 26-10-2007
Revised date: 19-5-2008
Accepted date: 11-6-2008

Please cite this article as: Calcagno, P., Chilès, J.P., Courrioux, G., Guillen, A., Geological modelling from field data and geological knowledge, Part I – Modelling method coupling 3D potential-field interpolation and geological rules, *Physics of the Earth and Planetary Interiors* (2007), doi:10.1016/j.pepi.2008.06.013

Geological modelling from field data and geological knowledge,

Part I – Modelling method coupling 3D potential-field interpolation and geological rules

P. Calcagno[1], J.P. Chilès[2], G. Courrioux[1], A. Guillen[1]

1. BRGM, 45060 Orléans Cedex 02, France
2. Ecole des Mines de Paris, 77300 Fontainebleau, France

Corresponding author: p.calcagno@brgm.fr, phone: +33 2 38 64 30 54, fax: +33 2 38 64 33 34

Abstract

An original method has been developed to model geology using the location of the geological interfaces and orientation data from structural field. Both types of data are cokriged to interpolate a continuous 3D potential-field scalar function describing the geometry of the geology. Geology contact locations set the position of reference isovalues while orientation data are the gradients of the scalar function. Geometry of geological bodies is achieved by discretising reference isovalues. Faults are modelled using the same method by inserting discontinuities in the potential field. Potential fields can be combined to model realistic, complex geometry: scalar functions representing separate geological *series* are merged automatically using geological rules to enable fast computation and easy update of interpretation. The methodology has been applied to a wide range of geological contexts including orogenic domains, basins, intrusive and extrusive environments.

Keywords

Geomodelling, 3D geology, geometric modelling, interface data, orientation data, potential-field interpolation, geological rules, geological pile, fault, fault network.

1. Introduction

The usefulness of 3D geometric models to better understand geology is now well established (Houlding 1994; Mallet 2002; Wijns et al.2003; Wu Qiang et al. 2005). Modelling consists in inferring a representation of the reality even where few data are available. This representation of the reality can be the final goal of modelling. Alternatively, the 3D geological model may be an input to simulations used to quantify physical processes. In both cases, inferring the geological formation at any location in 3D space is fundamental.

The appropriate methodology to develop a 3D model depends on the complexity of geology and on the available data. Existing methods often deal with 3D seismic data and are optimised for basin environment. In such a geological context, it may be sufficient to interpolate horizons. Where geology is cylindrical, and layered, 2D methods are adapted to construct horizons honouring cross-sections (Galera et al. 2003).

It is frequently the case, however, that available geological data are sparse, and nothing is known between over-sampled locations such as geological maps, cross-sections or boreholes. Moreover, geological bodies may have complex geometries derived from a long history of structural deformations. Classical structural measurements made in the field or by interpreting boreholes give the location of geological interfaces and the dip of the formations – the latter not necessarily located on the geological interface. However, apart from rare exceptions (e.g. de Kemp 2000), contact locations and tangency constraints only at contact points are taken into account to model the geometry of geology.

An original methodology has been developed to answer the following questions:

(i) How to infer the 3D geometry of geological bodies described only by sparse data?

(ii) How to take into account structural data measured on outcrops or in boreholes?

(iii) How to easily test alternative hypotheses to interpret complex geology?

By taking into account both contact locations and orientation data, coherent 3D models are constructed using a potential-field method to interpolate away from the data. Rules derived from the rock relationships between formations allow automatic building of the model, and facilitate its refinement and updating.

2. Potential-field interpolation method

The method developed here is based on three simple considerations:

(i) A geological interface delimits two geological formations.

(ii) Some orientation data sampled within geological formations are relevant to model the interfaces separating the formations.

(iii) The interfaces to be modelled may be regarded as belonging to an infinite set of surfaces aligned with the orientation field.

This situation is reasonably achieved in many geological situations:

- in sedimentary series, by considering a general parallelism between chronostratigraphic limits and stratigraphic planes;
- in igneous rocks, by using internal structures to determine pluton shapes;
- in metamorphic terrains, by assuming that the limit between two units displays a strong parallelism with metamorphic foliations.

Actually the method is very close to classical geological thinking in the sense that it attempts to reproduce the natural drawing of a geologist simultaneously guided by some observed contact points and by the knowledge of orientation field mentally inferred from structural data. This can be applied even if data are only known from field observations on topography.

The method can be used when the following two conditions are true:

I. Location of the geology interfaces is known at some places.

II. Orientation data are available. These sample the leading planar anisotropy of geological formations (stratification, schistosity or foliation), but are not necessarily located on geological interfaces. Polarity information is part of the orientation data. For example, in the case of a sedimentary series, polarity is the younging direction. For an intrusion, polarity is from the outside to the inside of the intrusion.

The basic method is designed to model a single geological interface or a series of subparallel interfaces $l_k = 1,2\ldots$ (Lajaunie et al.1997). Its principle is to summarise the geology by a *potential field*, namely a *scalar function* $T(p)$ of any point $p = (x, y, z)$ in 3D space, designed so that the interface l_k corresponds to an isopotential surface, i.e. the set of points p that satisfies $T(p) = t_k$ for

some unknown value t_k of the potential field. Equivalently, the geological formation encompassed between two successive interfaces l_k and $l_{k'}$ is defined by all the points p whose potential-field value lies in the interval defined by t_k and $t_{k'}$. In figurative terms, in the case of sedimentary deposits, T could be seen as the time of deposition of the grain located at p, or at least as a monotonous function of that geological time, and an interface as an isochronous surface, similarly to Mallet (2004). This figurative interpretation can be adequate in some applications but is not necessary for the development of the method.

Figure 1 illustrates this principle in two dimensions.

2.1. Data types

$T(p)$ is modelled with two kinds of data, as shown in Figure 1a:

(i) 3D points belonging to the interfaces $l_1, l_2, \ldots$; and

(ii) 3D unit vectors belonging to the orientation field of the interfaces and polarised along younging direction.

For the interpolation of the potential field, these data are coded as follows:

(i) Since the potential value at $m+1$ points $p_0, p_1, \ldots, p_m$ sampled on the same interface is not known, these data are treated as *m* increments $T(p_\alpha) - T(p'_\alpha),\ \alpha = 1, \ldots, m$, each one equal to 0. Two classical choices for p'_α consist in taking either the point p_0 whatever α, or the point $p_{\alpha-1}$ (the choice has no impact on the result; other choices are possible provided that the increments are linearly independent). Since the sampled data may be located on several interfaces, let M represent the total number of increments; M is equal to the total number of data points on the interfaces, minus the number of interfaces.

(ii) The polarised unit vector normal to each structural plane is considered as the gradient of the potential field. It therefore defines the value of the partial derivative $\partial T(p)/\partial u$ at the measurement point p_β in any direction u. The structural plane data at p_β is then expressed by three partial derivatives of the form $\partial T(p_\beta)/\partial u_\beta$, where u_β alternatively represents the three coordinate axes x, y, z. (Equivalently, another set of partial derivatives in three orthogonal

directions can be considered. For example, the polarised unit vector can be expressed by one partial derivative equal to 1 in the vector direction, and two partial derivatives equal to 0 in directions defining the structural plane.) Let N denote the total number of data of the form $\partial T\left(p_\beta\right)/\partial u_\beta$; in practice N is a multiple of 3 and the p_β form triplets of common points. Recall that the p_β do not necessarily coincide with the p_α; the latter are located on the interfaces whereas the former can be located anywhere.

2.2. Interpolation of the potential field

The potential field is then only known by discrete or infinitesimal increments. It is thus defined up to an arbitrary constant. So an arbitrary origin p_0 is fixed and at any point p the potential increment $T(p)-T(p_0)$ is kriged. The estimator is a cokriging of the form

$$T^*(p)-T^*(p_0)=\sum_{\alpha=1}^{M}\mu_\alpha\left(T(p_\alpha)-T(p'_\alpha)\right)+\sum_{\beta=1}^{N}\nu_\beta\frac{\partial T}{\partial u_\beta}(p_\beta)$$

where the weights μ_α and ν_β, determined in the cokriging system, are functions of p (and p_0). One may wonder why the potential increments are introduced to this estimator, given that their contribution is nil. The key reason is because the weights ν_β are different from weights based on the gradient data alone. These weights are constrained so that the interpolated field has same potential value at p_α and p'_α, which would not be the case, except by chance, if the potential increment data were not taken into account. Conversely, the gradient data also play a key role; because in their absence the estimator would be null anywhere.

Cokriging is performed in the framework of a random function model. $T(.)$ is assumed to be a random function with a polynomial drift

$$m(p)=\sum_{l=0}^{L}b_l f^l(p)$$

and a stationary covariance $K(h)$. Since the vertical usually plays a special role, the degree of the polynomial drift can be higher vertically than horizontally and the covariance can be anisotropic. For example, if we model several subparallel and subhorizontal interfaces, it makes sense to assume a

vertical linear drift of the form $m(p) = b_0 + b_1 z$, i.e. with two basic drift functions $f^0(p) \equiv 1$ and $f^1(p) = z$. A geological body with the shape of an ellipsoid would correspond to a quadratic drift, i.e. to the 10 basic monomial drift functions with degree less than or equal to 2. Note, however, that the drift function $f^0(p) \equiv 1$ shall be forgotten in any case since the potential increments as well as the partial derivatives filter b_0.

The use of cokriging requires a sound modelling of the joint spatial variations of the various variables. We are here in a favourable situation, since the second type of data — the partial derivatives — derive analytically from the potential field. The drift of $\partial T(p)/\partial u$ is therefore simply $\partial m(p)/\partial u$, i.e. a linear combination of the partial derivatives $\partial f^\ell(p)/\partial u$ with the same unknown coefficients b_ℓ as for $m(p)$, which allows an easy specification of the unbiasedness conditions. The covariances of partial derivatives are second-order partial derivatives of $K(.)$, and the cross-covariances of the potential field and partial derivatives are partial derivatives of $K(.)$, which enables the expression of the estimation variance and therefore its minimization. See section 5.5.2 of Chilès and Delfiner (1999) for further explanations.

2.3. Implementation of the cokriging algorithm

To guarantee the spatial continuity of the cokriging estimator, we use a unique neighbourhood, effectively including all data in the cokriging of $T(p)$ regardless of p. When we are not interested in the cokriging variance, cokriging is implemented in its dual form, which dramatically saves computing time (preliminary step: solving of one cokriging system with $L+M+N$ equations — typically up to several thousand equations — instead of an inversion of the cokriging matrix; cokriging at a target point: once the drift functions at the target point and the covariances between the target point and the data points have been computed, $2(L+M+N)$ arithmetic operations instead of $2(L+M+N)^2$). $T^*(p) - T^*(p_0)$ can be obtained at any point p. Its sign indicates if p is located in the older formation (negative value), in the younger one (positive value), or on the interface (null value). The latter property is used to display 3D views of the geological model with an algorithm generalising the marching cube (Lorensen and Cline 1987). It consists in starting from the estimation of $T(p) - T(p_0)$

at the nodes of a coarse regular grid and then requires intermediate points to be predicted to track the desired isopotential surface.

Since the cokriging is performed in unique neighbouring, solving the system in its dual form is the critical step for performances. The matrix size is linearly dependant to the square of number of data (number of potential increments plus partial derivatives plus drift functions). Lets' say that with a non-optimized standard linear system solver and a current PC (single processor, 3 GHz) it takes about one second to solve system with 400 data, one minute with 3000 data. So performances are becoming critical with amounts of data larger than a few thousands. These could be improved by adapting appropriate optimized covariances and solvers.

2.4. Choice of the covariance function and validation of the model

The choice of the covariance function $K(.)$ of the potential field is not obvious, because we are unable to compute a sample variogram of that potential field, for the simple reason that our sole data are increments with a zero value. Since we assume implicitly that the gradient exists, we know that covariance $K(.)$ is parabolic at the origin. The potential-field method can thus be used with an *a priori* covariance of that type. In that case, the interpolator shall be considered as a conventional one and cannot claim for optimality (from a geostatistical standpoint). Several checks on actual data sets have shown that covariances with a finite range give more sensible models than generalized covariances with an infinite range, and that a covariance such as the cubic model, which corresponds to a variable with partial derivatives at order 1 but not at order 2, works better than a highly regular covariance such as the Gaussian model. The method is therefore often used with a cubic covariance whose range is chosen by the user and sill is automatically fixed so that the covariance of the gradient is consistent with the experimental variance of the gradient data.

It is possible to do better by analysing the direct and cross variograms of the partial derivatives $\partial T(p)/\partial x$, $\partial T(p)/\partial y$, and $\partial T(p)/\partial z$, which can be experimentally calculated with the gradient data. Since the variograms of partial derivatives are second-order partial derivatives of the covariance of the potential field, their joint modelling amounts to modelling $K(.)$. This approach has been used by Aug (2004) — also see Chilès et al. (2006) — to two data sets in the French Massif Central. In both cases the final model was a sum of two or three anisotropic cubic covariances. This confirms the

interest in the cubic covariance model and calls for paying more attention to the anisotropy of the covariance.

The validation of the model can be done by discarding some data and trying to reconstitute them from the other data. It is also possible to apply the usual cross-validation method, which consists in deleting in turn one datum and estimating it from neighbouring data. A sound quantitative validation of course requires that the covariance model is not a simple *a priori* choice of the user but results from a fitting procedure.

2.5. Example

Sainte-Génis Mountain

The following example illustrates the modelling of a folded structure in the Subalpine chains, S-E France. The study area, located in the western Baronnies, and known as Sainte-Génis Mountain, is an E-W elongated syncline with a core of lower Cretaceous, filling a structural depression. This is a typical example of a preliminary model realised using only standard data from field observation and geological map (Figure 2). Relevant geological contacts are digitised from the geological map or from field observations. Structural dips are also extracted from the map and supplemented with additional field measurements in order to achieve a widespread sampling of orientation data. For this model, all Mesozoic interfaces are assumed to be nearly parallel at the modelling scale. The Sainte-Génis modelling demonstrates the advantage of this approach, whereby a lack of data on some interfaces within some areas is compensated by data on other interfaces in other areas.

3. Taking faults into account

There are three aspects regarding the modelling of faults. (i) modelling the fault geometry as a surface, (ii) describing how faults terminate in 3D space, and (iii) defining the way in which they impact geological interfaces.

3.1. Fault geometry

Fault interpolation is performed in the same manner as for geological interfaces: one interpolates a potential field using fault traces as data points and fault orientation data as gradients. Thus, each fault

is determined from its own potential field. The geometry of the fault is defined by the corresponding isosurface extracted from the fault potential-field.

A useful query with respect to faults is to know on which side of the fault is a given point p. Using the implicit representation of the fault, the answer is straightforward: point p is either on the foot wall or hanging wall depending on whether the value of the fault potential-field at point p is smaller or larger than the fault isovalue. By convention, the hanging wall and foot wall are defined in accordance with the orientation of the gradient data. Consequently, it is easy to implement a function determining if a fault occurs between two points p_1 and p_2.

3.2. Fault border

Infinite and finite faults

Faults can be considered as infinite (relative to the study area), or finite. For the latter case we must define the extent of the fault. Since it is rare to have actual observations defining the tip line of a fault (i.e. the limit where no more displacement occurs), we choose to define this boundary as circular or elliptic. We consider that the fault extent are defined by the intersection of the potential-field isosurface and a sphere (or an ellipsoid) of given radius centred on the data defining the fault.

Fault network

A fault may also terminate against another fault. A *fault network* is defined as a set of faults f_n and a set of fault-fault relations ($f_i \rightarrow f_j$) (Figure 3a). Using the isopotential representations of the various faults and taking the fault network relations into account, it is possible to identify the valid and invalid portions of (fault) isopotential surfaces, and so achieve a network of fault surfaces that respects the fault-fault relations (Figure 3b).

3.3. Fault influence

Taking faults into account for interpolating geological interfaces is achieved by adding discontinuous drift functions into the cokriging system. These spatial functions model the shape of the influence of the fault.

For the simplest case of an infinite fault with rigid translation, one assumes a fixed discontinuity of the potential field when crossing the fault; the drift function is equal to 0 on one side of the fault and to 1

on the other side (Figure 4a). The value of this discontinuity is determined automatically by the cokriging process using the implicit representation of the fault as explained in 3.1.

In the case of a finite fault, the value of the associated drift function is $+1$ at the centre-point on one side and respectively -1 at the centre on the other side. The amplitude of the drift function then progressively decreases to 0 on one side, respectively increases to 0 on the other side, where the influence of the fault vanishes (Figure 4b).

Figure 5 illustrates the effect of varying fault 'radius' on interface modelling. If fault extents are defined in terms of an elliptical shape, the spatial function is computed by applying similar rules with an anisotropic distance.

For a *fault network* the spatial function is designed as follows: each fault has its own function with the same rules as for finite or infinite faults, except that it is set to 0 as soon as it crosses a fault against which it stops (Figure 4c). Note that each interface has to be known at, at least, one 3D point within each fault block.

3.4. Example

Limagne

The Limagne d'Allier basin is located in an area where the temperature at 5 km depth is high. The area has been studied for its geothermal potential (Genter et al. 2005).

Located north of Clermont-Ferrand, France (see map on Figure 6 for location), this N-NE to N-S oriented Tertiary basin is bounded by regional faults. From Upper Eocene to Oligocene, a graben formed due to progressive subsidence resulting from the extension phase affecting the West-European plate. The Limagne basin is delimited by the Clermont-Ferrand fault in the east and by the Aigueperse fault in the north. Both faults have a normal throw of several hundred metres, with a strike slip component for the Aigueperse fault. The combination of those two faults creates the deepest part of the basin situated around Riom city. Based on seismic lines interpretation, most of the faults inside the basin had no activity after the Oligocene. The two main faults, however, do show evidence of later movement.

Figure 6 shows the geometry of the basement built using a fault network and drift functions for the faults. Geological contacts and orientation data were determined from field observations, seismic sections and boreholes, together with interpretive data for the basement surface derived from

gravimetric inversion. The relative displacements of the fault blocks were constrained by basement interface location on both sides of each fault.

The Limagne example is further developed in Section 4.3.

4. Generalisation of the modelling method by combining multiple potentials

The potential-field interpolation method described in Section 2 assumes that the entire area can be modelled as geological interfaces belonging to a series of sub-parallel surfaces aligned with the orientation field. This hypothesis implies that interfaces always exist throughout the domain. By definition, two consecutive isosurfaces of a potential field can never intersect or tangent each other but have a sub-parallel geometric relationship (Figure 1b).

Apart from occasional sedimentary examples, a geological body rarely exists throughout a domain. Geological events usually lead to complex topology where formations cut across or onlap onto each other as a result of deposition, erosion, intrusion or hiatus. Such geology can be modelled by combining multiple potential fields.

4.1. Combination of potential fields

The core of the method consists in using geological rules to combine various potential fields:

R1. Interfaces of geological formations having sub-parallel behaviours are grouped together into *series*. A single potential field is used to model a *series*.

R2. A chronology defines the time-order of *series* within the model.

R3. A relationship is defined for each *series* to drive its (modelling) behaviour with respect to the chronologically older ones.

Concerning R3, two basic relationships are defined to specify how a *series* impacts on a model: (i) the *Erode* relation allows *series* to occur and truncate, or cut across, older ones, (ii) the *Onlap* relation enables the *series* to be present only where space is available without changing the geometry of the older *series*. Figure 7 describes a synthetic example with 3 *series*; each one consists of a single geological formation. This figure shows the importance of the *series* chronology and the consequence of their relationships on the modelled geometry.

R1, R2 and R3 define a *geological pile*: a set of geological formations, chronologically ordered, gathered together in interacting *series*. The knowledge contained in the *geological pile* defines the topology of the model. It enables to automatically merge the various scalar functions interpolating the *series* and thus to achieve the geometry of a coherent complex 3D model.

Let's assume that I *series* describe the geology of the domain. I potential fields are used to model the *series*. The corresponding scalar functions T_i, $i = 1,2 \ldots I$ are defined in the whole 3D space and I values $T_1(p), T_2(p), \ldots, T_I(p)$ are associated to a given 3D point $p(x, y, z)$. The combination method consists in partitioning the 3D space in areas where a given scalar function is valid, i.e. in identifying, among the T_i, the scalar function T_p to consider for p. Finally, the geological formation associated to p is deduced from T_p by using the methodology described in Section 2. The comparison method depends on the chronological order of the scalar functions and on the relationship *Erode* or *Onlap* associated to T_i.

4.2. Faults

For the case of multiple potential fields, faults are managed according to the rules described in Section 3. Based on field observations of the relationship between geological formations and faults, each (geological) potential field has its own faults subset taken among the general set of faults for the model. Thus, a fault may affect all geological formations of a *series* but will have no effect on the geological formations of another *series*.

4.3. Example

Limagne

Let's resume the example introduced in Section 3.4.

Overlying the Limagne d'Allier basement, four main sedimentary sequences fill the basin: Middle Eocene (S1), Upper Eocene (S2), Rupelian (S3) and Chattian (S4). Each sequence is composed of a sedimentary cycle ranging from detrital formations at the base ("Reservoir"), followed by alternating layers of detrital and carbonate sediments ("Intermediate"), and capped by formations of marls and carbonates at the top ("Top"). In order to model the erosional surfaces that define top of each sedimentary cycle, the top of marls and carbonates for each sequence is assigned to an *Erode*

relationship in the *geological pile* (Figure 8). The thickness of each formation varies both spatially and temporally. The “Reservoir” formations are thicker along the basin-margins than in the centre of the basin. The “Intermediate” formations correspond to a transitional environment, and lacustrine carbonate formations are thicker in the central, deeper part of the basin. Since the thickness variability is not correlated from one formation to another within the same sequence, their interfaces cannot be represented by isovalues of a single potential field. Consequently, each formation must be modelled with an independent potential field (Figure 8).

The resulting model is illustrated in Figure 9 showing a 3D view of the “Reservoir” formations, the boreholes and two orthogonal sections (Figure 9a), and a W-E section of the whole basin (Figure 9b). The modelled cross-section demonstrates (i) how the fault network controls the fault system geometry (see Section 3.2), (ii) the outcomes of the *Onlap* or *Erode* rock relationships (see Section 4.1), and (iii) the implications of the relations between faults and series (see Section 4.2).

5. Discussion

The major feature of this original modelling method consists in describing the 3D geological space through a continuous potential-field scalar function T where geological boundaries are reference isopotential surfaces and structural dips define gradients of the scalar function. As the method results in a continuous model within the domain, the geological formation at any 3D point $p=(x,y,z)$ is implicitly defined by the value $T(p)$. This fundamental capability is used to explicit — by interrogating the potential field — so as to visualise the model in 1D along a borehole or a tunnel, in 2D on a map or section and as 3D surface shapes and volumes. This property can be exploited to export the model on any wireframe meshes.

The spatial continuity of the potential field is ensured by implementation of the cokriging using a unique neighbourhood approach. Although a coherent 3D model is constructed, the dual cokriging implementation implies that the computing time needed to interpolate at a given point is directly proportional to the number of data plus drift functions. Increasing the number of data also increases the size of the system to be solved in the preliminary step. This presently limits the number of data to several thousand. Such a limit could be avoided (i) by using local neighbourhoods, with a damping factor for distant data points in order to maintain the continuity of the interpolator, following an

approach developed by Gribov and Krivoruchko (2004) for simple kriging, or (ii) by solving the cokriging system more efficiently using covariance tapering to simplify the scalar function matrix (Furrer et al. 2006, also in the case of simple kriging).

A particular attention has to be paid to the data and interpretation input in the model. As the work presented here is well adapted when only a few data are available, it is far better to input only real observation from the field, or from boreholes, and to use the modelling as a help for interpretation. The result of such a preliminary model can be discussed and refined by returning in the field to acquire new data at strategic places and/or by adding geologist own interpretation. For instance and as far it is possible, authors would recommend to use outcrop measurements instead of digitized geological map to avoid artefacts from the interpreted map that is already a model. However, input of interpreted data where observation are missing, e.g. seismic lines, are of a great help in creating the model but can be checked and re-interpreted if necessary, depending on their interaction with the model proposed only using the observed data.

The way of acquiring data in the field has to be adapted to the scale of the model. Such as for geological mapping, a regional scale model, e.g. a few tens of kilometres wide, would not describe microstructures observed on the outcrop. As the model will benefits from a regular outcrop sampling adapted to the model scale, it is important to input measurements even if they are constant. For example, the measurements showing a same dip for a given formation on successive outcrops have to be used to better constrain the model.

Various orientation data may be measured in the field, e.g. S_0, S_1, S_2, etc. However the ones that are taken into account for the model have to be representative of the geological interfaces, either they are measured on or outside the contact.

Automatic construction of the model is achieved using the geological knowledge input in the *geological pile.* In that case, multiple *series* are combined to model geology. One can add new data or update an interpretation without consideration of the implications for the geometry of formations since the rules of the *geological pile* automatically manage the result. The interpreter may also revise the *geological pile* itself to test alternative interpretations of the chronology of geological events or different rock relation between formations. Strictly the same data, but combined to a revised *geological pile*, will generate a different model outcome.

The basic relationships of the series — *Erode* and *Onlap* — can be combined to define other relationships to model specific geological bodies, such as an intrusion. In that case, the *Intrusion* relationship can be defined as the combination of (i) an *Erode* sequence using a polarity directed toward the inside of the intrusive body in order to erode the existing bedding and (ii) an *Onlap* sequence to fill the intrusive body. Figure 10 shows a synthetic example of an intrusive body modelling.

The modelling method requires that geological data be managed in a way whereby they represent the relevant geological interfaces. For instance, limits between geological formations in boreholes (deviated or not) have to be transformed into geological interface points. Note that a boundary between two formations is not necessarily assigned to the base or the top of one of the two formations if an erosion sequence or a hiatus occurred during the geological history. Figure 11 illustrates a case where a formation is not encountered in a borehole, either the formation was not deposited, or the formation has been eroded and replaced by a younger one. As shown in Figure 11, knowledge of the rock relationships defined in the *geological pile* can be used to unequivocally assign the correct geological interface to drilled interval boundaries in a borehole.

The same procedure can be applied to GIS polygons representing a geological map; the curve separating two geological formations is not necessarily the base or the top of one of the two formations. In similar manner to the borehole case illustrated above, given any two adjacent formations observed in geological mapping, the rules contained in the *geological pile* can be used to automatically assign the correct geological interface to the mapped contact, and so to derive a valid geological model.

The potential-field interpolation method with the associated rules of the *geological pile* has been successfully applied to various geological contexts, including:

(i) orogenic domains (Courrioux et al. 2001, Maxelon et al. 2005, Marquer et al. 2006, Putz et al. 2006, Calcagno et al. 2007);
(ii) intrusive environments (Faure et al. 2001, Martelet et al. 2004, Talbot et al. 2004, Joly 2007);
(iii) basins (Calcagno et al. 2004, Genter et al. 2005);
(iv) mining geology (Burtt et al. 2005, McInerney et al. 2005);
(v) geotechnics (Strzerzynski et al. 2005, Calcagno et al. 2006).

6. Conclusion

The method presented in this paper is dedicated to 3D geological models building from interface points and polarised orientation data. The methodology is designed for cases where the geology is only known at sparse locations, e.g. when data are available on the field but not at depth. A wide range of geological contexts can be tackle such as orogenic domains, basins, intrusive domains as long as the available data are located on map, sections or boreholes. The orientation data, i.e. dip measurements, are not necessarily located on the geological interfaces. They can represent stratifications or foliations related to the contacts. Data are interpolated through a potential field continuously defined in the entire 3D domain. Thus, the model allows to assign the geological formation at any 3D point. That property makes possible to export the geometry to various meshes. Figure 12 synthesises this methodology for geological modelling. Geological interfaces are particular isosurfaces extracted from the potential field. They may have any kind of 3D geometry: multilayer type, recumbent folds, complex intrusions, etc. The geometry of faults is computed by applying the same method. Faults can be infinite within the 3D domain, interrelated in a fault network or finite. Geological rules are defined to model complex geology where formations onlap onto or erode another. These rules are also used to automatically assign the right geological interface between two consecutive formations. That methodology automatically provides the intersections between geological bodies; allowing fast modelling and giving the geologist the opportunity to focus on geological interpretation. As the *geological pile* defines the topology of the model, one can modify it without changing the data to produce alternative interpretations leading to alternative geometries. This capability also make possible to update the model when new data or interpretation is available.

The work presented in this paper is implemented in *3D GeoModeller* package designed for geological interpretation and development of 3D geological models (http://www.geomodeller.com and http://3dweg.brgm.fr).

A complementary methodology has been developed to validate a geological model by forward modelling and inversion of geophysical data. This methodology is described in another paper of this

special issue: *Geological modelling from field data and geological knowledge, Part II – Modelling validation using gravity and magnetic data inversion* (Guillen et al.).

Acknowledgements

Dimitri Schreiber did the Sainte-Génis Mountain modelling at Geosciences Azur (Nice, France). The Limagne model was performed at BRGM by Adrien Dagallier and supervised by Albert Genter. Thank you all at Intrepid Geophysics (*3D GeoModeller* software distributor) and especially Phil McInerney and Desmond Fitzgerald for their help including the English review of the manuscript. Authors thank Guillaume Caumon, Cees Passchier and the anonymous reviewer for their fruitful comments.

References

Aug, C., 2004. Modélisation géologique 3D et caractérisation des incertitudes par la méthode du champ de potentiel. Doctoral thesis, E.N.S. des Mines de Paris, 198 pp.

Burtt, A., Williams, H., Calcagno, P., 2005. Reawakening the Curnamona Province — a 3D perspective. South Australian Resources and Energy Investment Conference, Adelaide.

Calcagno, P., Lazarre, J., Courrioux, G., Ledru, P., 2007. Modélisation 3D d'un domaine orogénique externe : Le massif de Morges, Pelvoux (Alpes occidentales). Bulletin de la Société Géologique de France 178, 26 274.

Calcagno, P., Courrioux, G., Guillen, A., Fitzgerald, D., McInerney, P., 2006. How 3D implicit geometric modelling helps to understand geology: The 3DGeoModeller methodology. Int. Assoc. for Mathematical Geology XIth International Congress, Université de Liège, Belgium.

Calcagno, P., Thinon, I., Courrioux, G., Guillen, A., Guenoc, P., 2004. 3D geometric modelling: A tool for margin and basin interpretation illustrated with the eastern Corse case-study (NW Mediterranean sea). RST, Joint Earth Sciences Meeting, Société Géologique de France — Geologische Vereinigung, Strasbourg.

Chilès, J.P., Aug, C., Guillen, A., Lees, T., 2006. Modelling the geometry of geological units and its uncertainty in 3D from structural data: The potential-field method. In Orebody modelling and strategic mine planning — Uncertainty and risk management models. Spectrum Series 14, Australasian Institute of Mining and Metallurgy, Carlton, Victoria, 329-336.

Chilès, J.P. and Delfiner, P., 1999. Geostatistics: Modeling Spatial Uncertainty. John Wiley & Sons, New York, NY.

Courrioux, G., Nullans, S., Guillen, A., Boissonnat, J.D., Repusseau, P., Renaud, X., Thibaut, M., 2001. 3D volumetric modelling of Cadomian terranes (Northern Brittany, France); An automatic method using Voronoi diagrams; The Cadomian crust of Brittany (France); 3D imagery from multisource data (GeoFrance 3D). Tectonophysics 331, 181-196.

de Kemp, E.A., 2000. 3-D visualization of structural field data: Examples from the Archean Caopatina formation, Abitibi greenstone belt, Quebec, Canada. Computers & Geosciences 26, 509-530.

Faure, M., Charonnat, X., Chauvet, A., Chen, Y., Talbot, J., Martelet, G., Courrioux, G., Monie, P., Milesi, J., 2001. Tectonic evolution of the Cevennes para-autochthonous domain of the Hercynian French Massif Central and its bearing on ore deposits formation. Bulletin de la Société Géologique de France 172, 687-696.

Furrer, R., Genton, M.G., Nychka, D., 2006. Covariance tapering for interpolation of large spatial datasets. Journal of Computational and Graphical Statistics 15 (3), 502-523.

Galera, C., Bennis, C., Moretti, I., Mallet, J., 2003. Construction of coherent 3D geological blocks. Computers & Geosciences 29, 971-984.

Genter, A., Giot, D., Guillou-Frottier, L., Calcagno, P., Courtois, N., Courrioux, G., Dagallier, A., Giraud-Petelet, E., Goyeneche, O., Lieutenant, N., Martelet, G., Negrel, P., Rocher, P., Serra, H., Serrano, O., Laplaige, P., 2005. Low to medium temperature geothermal resources in the Limagne basin (France). Proceedings World Geothermal Congress 2005. Antalya, Turkey, 24-29 April 2005.

Gribov, A. and Krivoruchko, K., 2004. Geostatistical mapping with continuous moving neighbourhood. Mathematical Geology 36, 267-281.

Guillen, A., Calcagno, P., Courrioux, G., Joly, A., Ledru, P., Geological modelling from field data and geological knowledge, Part II – Modelling validation using gravity and magnetic data inversion. This issue.

Houlding, S.W., 1994. 3D Geoscience Modeling; Computer Techniques for Geological Characterization. Springer-Verlag, Berlin, Germany.

Hurtig, E., Cermak, V., Haenel, R., Zui, V., 1991. Geothermal Atlas of Europe: Hermann Haack Verlagsgesellshaft. 156 pp.

Joly, A., 2007. Relations plutons et discontinuités lithosphériques. Approche pluridisciplinaire de la mise en place de plutons granitiques le long du Sillon houiller (Massif Central Français). Doctoral thesis, Université d'Orléans, 304 pp.

Lajaunie, C., Courrioux, G., Manuel, L., 1997. Foliation fields and 3D cartography in geology; principles of a method based on potential interpolation. Mathematical Geology 29, 571-584.

Lorensen, W.E. and Cline, H.E., 1987. Marching Cubes: A high resolution 3D surface construction algorithm. Computer Graphics, 21(4), 163-169.

Mallet, J.L., 2004. Space-time mathematical framework for sedimentary geology. Mathematical Geology 36, 1-32.

Mallet, J.L., 2002. Geomodeling. Oxford University Press, Oxford, New York.

Marquer, D., Calcagno, P., Barfety, J., Baudin, T., 2006. 3D modeling and kinematics of the external zone of the French western Alps (Belledonne and Grand Chatelard massifs, Maurienne valley, Savoie). Eclogae Geologicae Helvetiae 99, 211-222.

Martelet, G., Calcagno, P., Gumiaux, C., Truffert, C., Bitri, A., Gapais, D., Brun, J.P., 2004. Integrated 3D geophysical and geological modelling of the Hercynian suture zone in the Champtoceaux area (South Brittany, France). Tectonophysics 382, 117-128.

Maxelon, M. and Mancktelow, N.S., 2005. Three-dimensional geometry and tectonostratigraphy of the Pennine zone, central Alps, Switzerland and northern Italy. Earth-Science Reviews 71, 171-227.

McInerney, P., Guillen, A., Courrioux, G., Calcagno, P., Lees, T., 2005. Building 3D geological models directly from the data? A new approach applied to Broken Hill, Australia; Digital Mapping Techniques '05; Workshop Proceedings. Open-file report — U.S.Geological Survey OF 2005-1428, 119-130.

Putz, M., Stuwe, K., Jessell, M., Calcagno, P., 2006. Three-dimensional model and late stage warping of the Plattengneis shear zone in the eastern Alps. Tectonophysics 412, 87-103.

Strzerzynski, P., Guillot, S., Courrioux, G., Leloup, H., Ledru, P., Darmendrail, X., 2005. Integrative 3D geological modelling along the Lyon Turin railway project (internal Briançonnais domain of the western Alps). Geoline 2005, Lyon, France.

Talbot, J.Y., Martelet, G., Courrioux, G., Chen, Y., Faure, M., 2004. Emplacement in an extensional setting of the Mont Lozere-Borne granitic complex (SE France) inferred from comprehensive AMS, structural and gravity studies. Journal of Structural Geology 26, 11-28.

Wijns, C., Boschetti, F., Moresi, L., 2003. Inverse modelling in geology by interactive evolutionary computation. Journal of Structural Geology 25, 1615-1621.

Wu, Q., Xu, H., Zou, X., 2005. An effective method for 3D geological modeling with multi-source data integration. Computers & Geosciences 31, 35-43.

Figures captions

Figure 1.

Principle of the potential-field interpolation method (in 2D).

(a) A geological formation mapped by the position of its interfaces with two other formations (red points and blue points) and dip measurements (dip symbols).

(b) The geological formation modelled by potential-field method. Red and blue curves represent the reference isovalues of the modelled geology contact interfaces. White curves are selected isovalues of the potential field; in geological terms these may be 'trends' or foliations trajectories. The geological interfaces honour both contact points and orientation vectors.

Figure 2.

Sainte-Génis Mountain 3D geological model. The Mesozoic geological interfaces are modelled by isovalues of a potential field.

(a) Geology contact data points (crosses linked by segments) and orientation data (dip symbols) observed in the field.

(b) 3D view of the geological model, looking S-W.

(c) Modelled geology on section S-N.

Figure 3.

Example of a fault network showing selected faults terminating against other faults.

(a) Table describing the topology of the relations between faults: f1 stops on f2; f1 stops on f4; f3 stops on f6; f5 stops on f4; f6 stops on f2.

(b) Geometry of the fault network.

Figure 4.

Graphical depiction of the drift function introduced into the cokriging equations in order to implement the effect of offsets to geological formations across faults.

(a) Infinite. The drift function is 1 on one side of the fault and 0 on the other side (transverse profile). The longitudinal profile shows that the fault is infinite.

(b) Finite. The domain of influence is an ellipsoid. The drift function varies from 1 or -1 to 0 when moving away from the fault (transverse profile). Along the fault, the drift function decreases from the centre to the fault limits (longitudinal profile).

(c) Fault network. A fault network comprised of an infinite (f2) and a semi-infinite fault (f1) which use drift functions of the type shown in (a). The network partitions 3D space in fault blocks. The value (0 or 1) of the drift function for each bounding fault is noted.

Figure 5.

Geometry of the fault depends on the drift function radius. Red crosses are geology contact points for the modelled geological interface. Green crosses are data defining the position of the fault.

(a) Infinite fault.

(b) Finite fault. $Radius = 500.$

(c) Finite fault. $Radius = 400.$

(d) Finite fault. $Radius = 300.$

Figure 6.

View to the N-W of the 3D geological model of the basement below the Limagne basin, illustrating the network of faults used to model the basement structure (model dimensions: 30 km x 35 km x 5 km). The geometry of the basement was modelled by taking into account field geology observations, seismic sections and boreholes together with a basement surface derived from gravimetric inversion. The location map shows contours of temperature extrapolated to 5 km depth (Hurtig et al. 1991); the Limagne basin project (star) is located in an area of anomalously high temperature.

Figure 7.

Complex geology is modelled using different potential-field functions for different geological series. These multiple potential fields are managed using *Onlap* and *Erode* relations between *series*. In this example each *series* comprises a single formation.

(a) Interpolated Formation 1 (basement) and data for potential field of Formation 2.

(b) Formation 2 interpolated using an *Onlap* relation and data for potential field of formation 3.

(c) Formation 3 interpolated using an *Erode* relation.

Figure 8.

The *geological pile* for the 3D model of the Limagne basin project is derived from the broad geological knowledge of the basin. Four sedimentary sequences (S1 to S4) are deposited on top of the basement. Each sequence is divided into three depositional phases (“Reservoir”, “Intermediate” and “Top”). The sequences are separated by erosional surfaces (*Erode* relation for the top series of the four sequences). Each formation is modelled using independent potential fields because the variability of thickness is not correlated from a formation to another.

Figure 9.

View of the Limagne basin geology model (30 km x 35 km x 5 km). See Figure 8 for formations list and colour.

(a) 3D view from S-E of the 4 detrital formations (“Reservoir”) volumes in the central part of the model along with the boreholes in the area and two cross-sections (S-N and W-E).

(b) W-E section of the whole basin. (1) A fault stopping on another one according to the fault network. (2) *Onlap* deposition of S3_Reservoir_Series on S2_Top_Series (3) *Erode* relation of S1_Top_Series makes an erosional surface between sequence S1 and S2. (4) Fault impacts S2_Intermediate_Series. (5) S3_Top_Series is not affected by the fault.

Figure 10.

Intrusion modelling presented on a synthetic example. The *Intrusion* relationship is the combination of an *Erode* sequence eroding the bedding *series*, followed by an *Onlap* sequence filling the intrusive body. Note that the polarity of the orientation data of the intrusive body is directed towards the inside of the body.

(a) Data presented on a section.

(b) *Geological pile* of the model.

(c) The intrusive body visualized in 3D and the bedding displayed on a cross-section.

Figure 11.

How to determine valid geology contacts from borehole intervals?

(a) Consider three formations A (oldest), B, and C (youngest). B is missing in the central borehole. The issue is to define a geological evolution to determine which interface separates A and C.
(b) B is missing because of an erosion episode between B and C deposition. In such a geological hypothesis, the historical top of A has been eroded. The boundary between intervals A and C must be assigned to an erosion surface. This is also the case for the boundary between B and C in the lateral holes. On the other hand, the boundary between intervals A and B corresponds to the historical top of A.
(c) B is missing because it was never deposited. For this case, the boundary between intervals A and C is a point belonging to the historical top of formation A. In the two other holes, each boundary between intervals is also the historical top of the lower interval.

Figure 12.
3D geological modelling methodology.
The 3D geological model is built from contact points and orientation data by using geological rules and knowledge. The potential-field interpolation method delivers a model defined continuously in 3D. Consequently, the geological formation can be inferred at any 3D point of the studied space. This capability facilitates 1D, 2D and 3D visualisation of the model, and export of model maps, surfaces, volumes and meshes.

Figure1

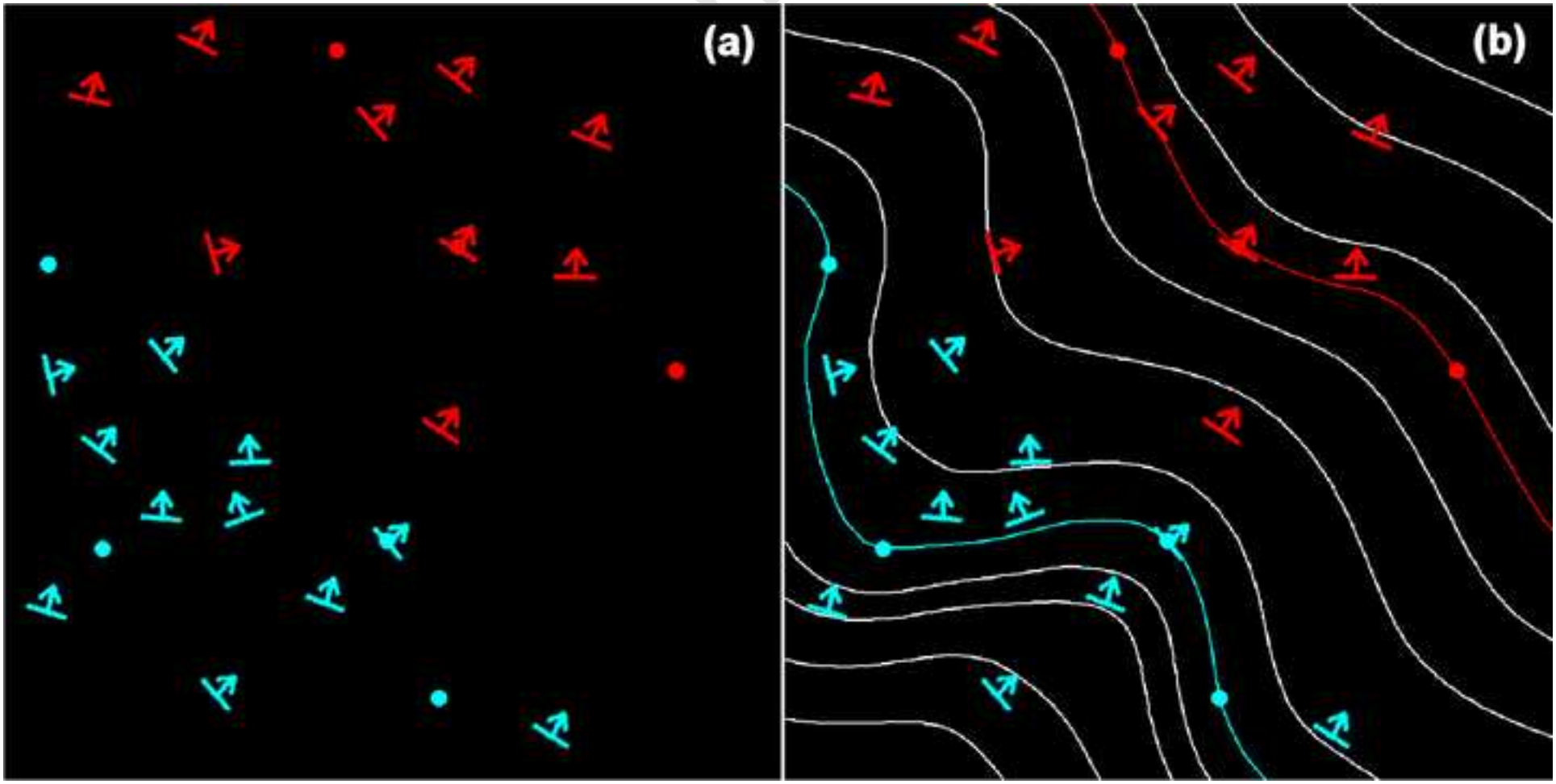

Figure2

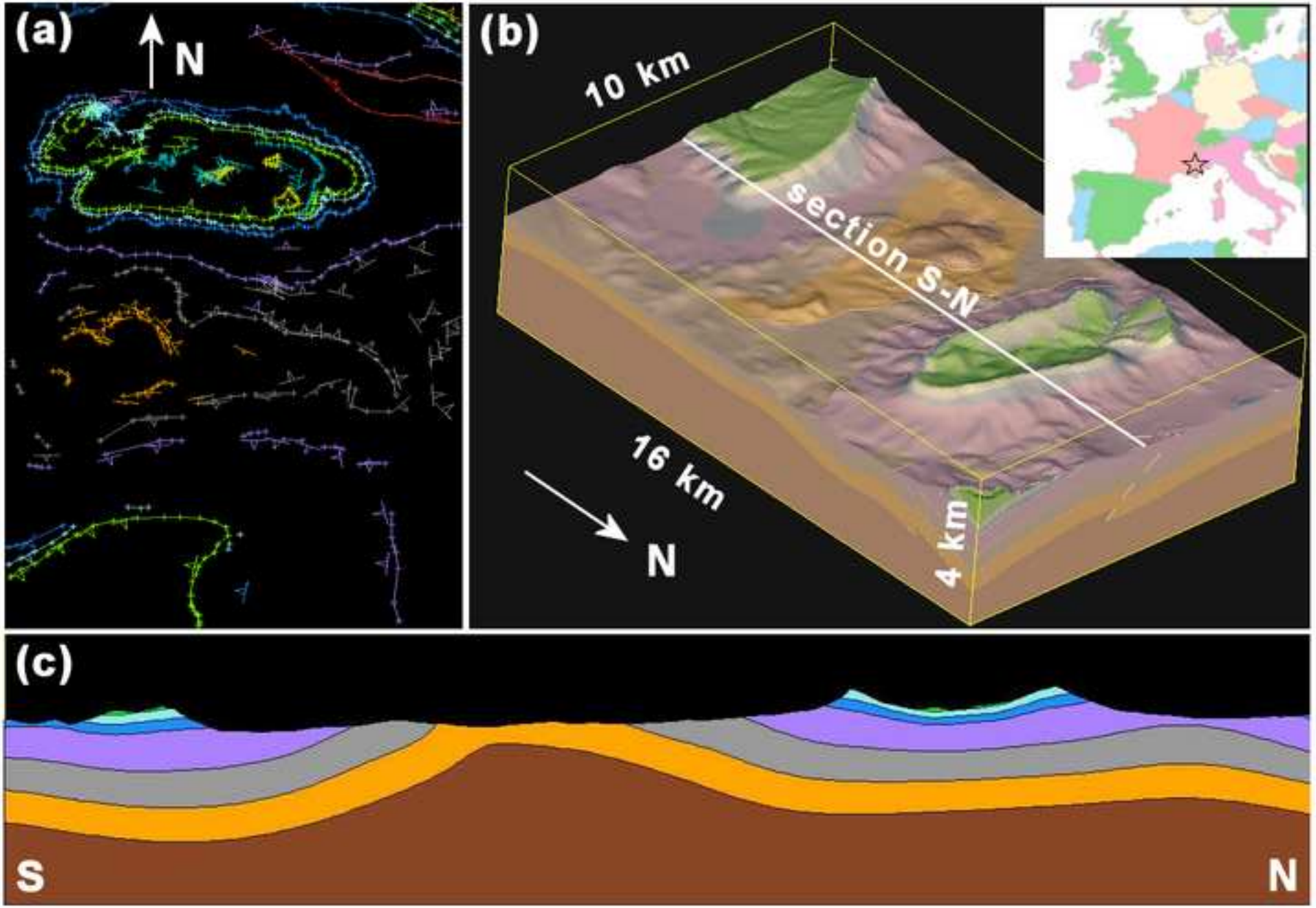

(a)

Stops on ↱	f1	f2	f3	f4	f5	f6
f1		X		X		
f2						
f3						X
f4						
f5				X		
f6		X				

(b)

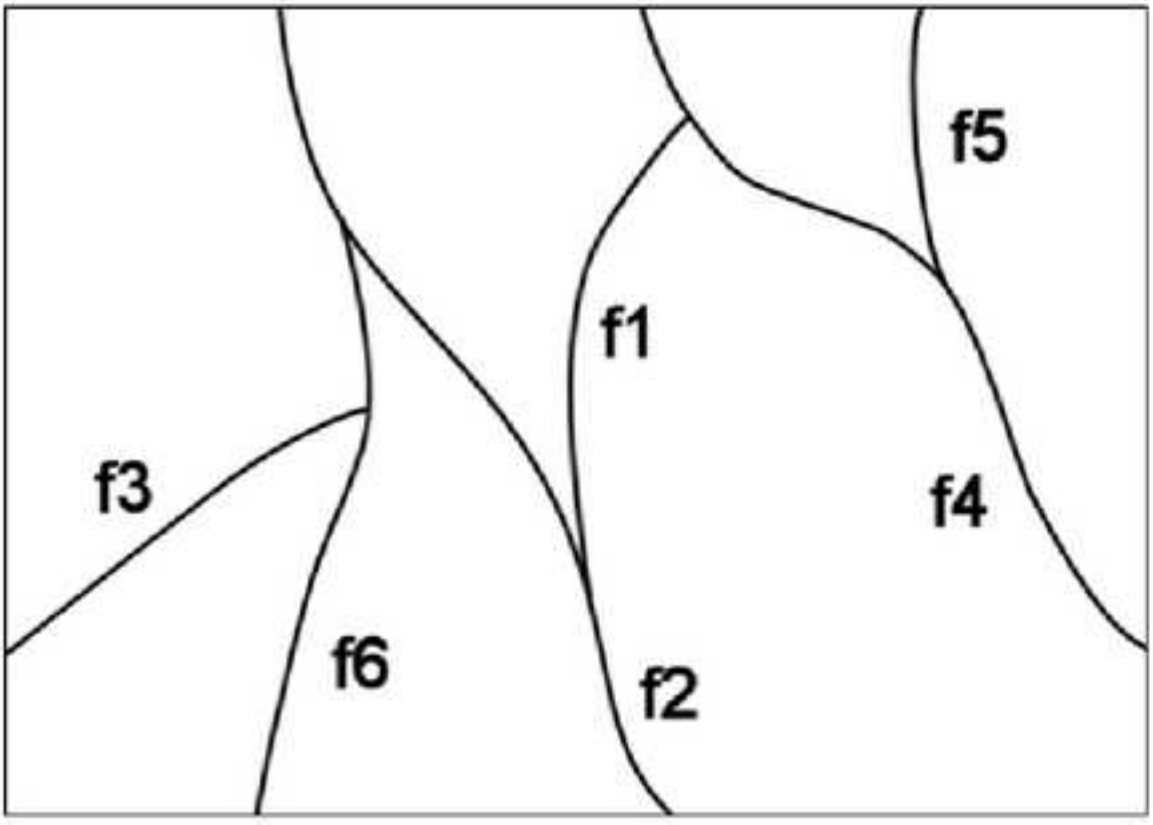

Figure4

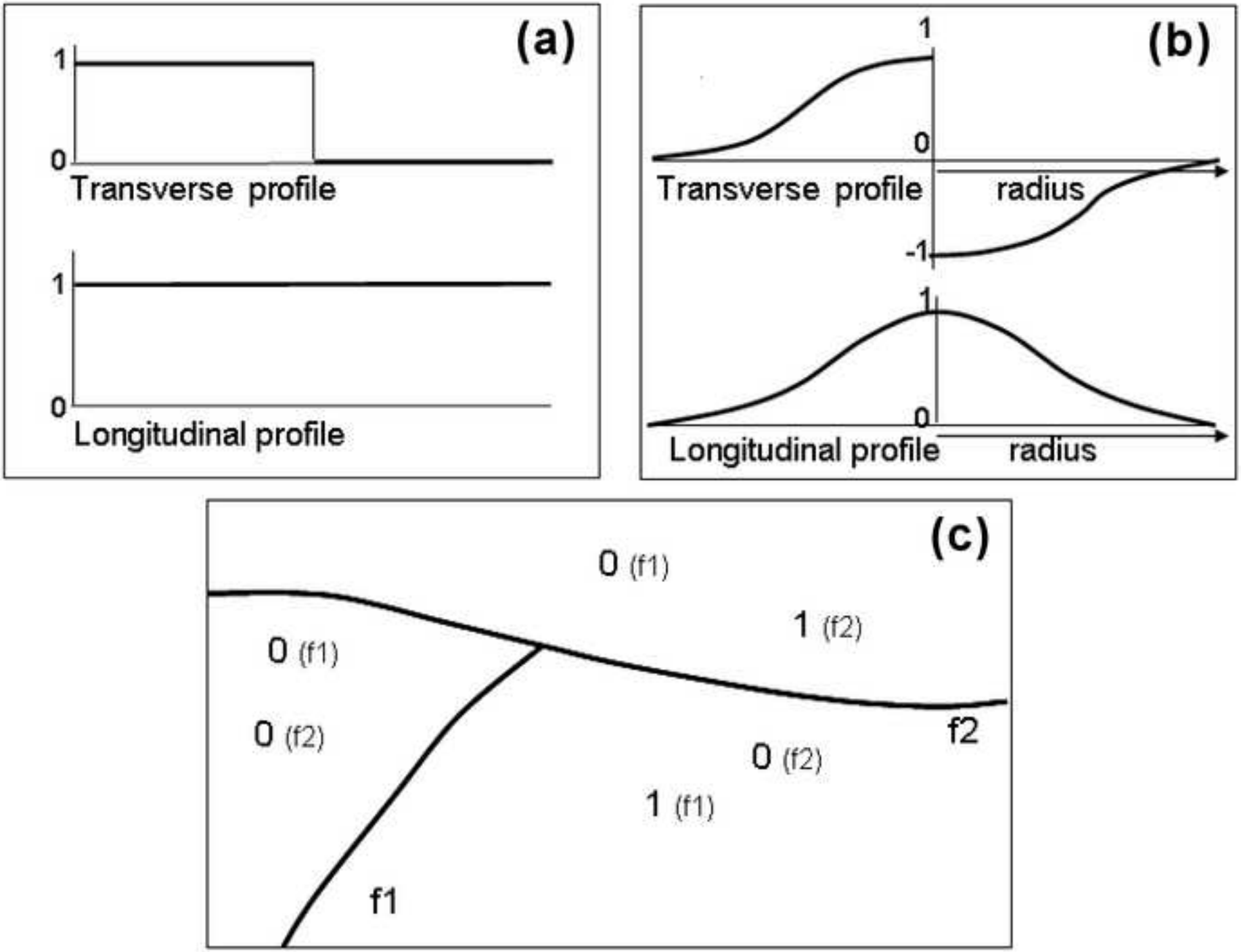
(a)
1
0
Transverse profile
1
0
Longitudinal profile
(b)
1
0
-1
Transverse profile
radius
1
0
Longitudinal profile
radius
(c)
0 (f1)
1 (f2)
0 (f1)
0 (f2)
f2
0 (f2)
1 (f1)
f1

Figure5

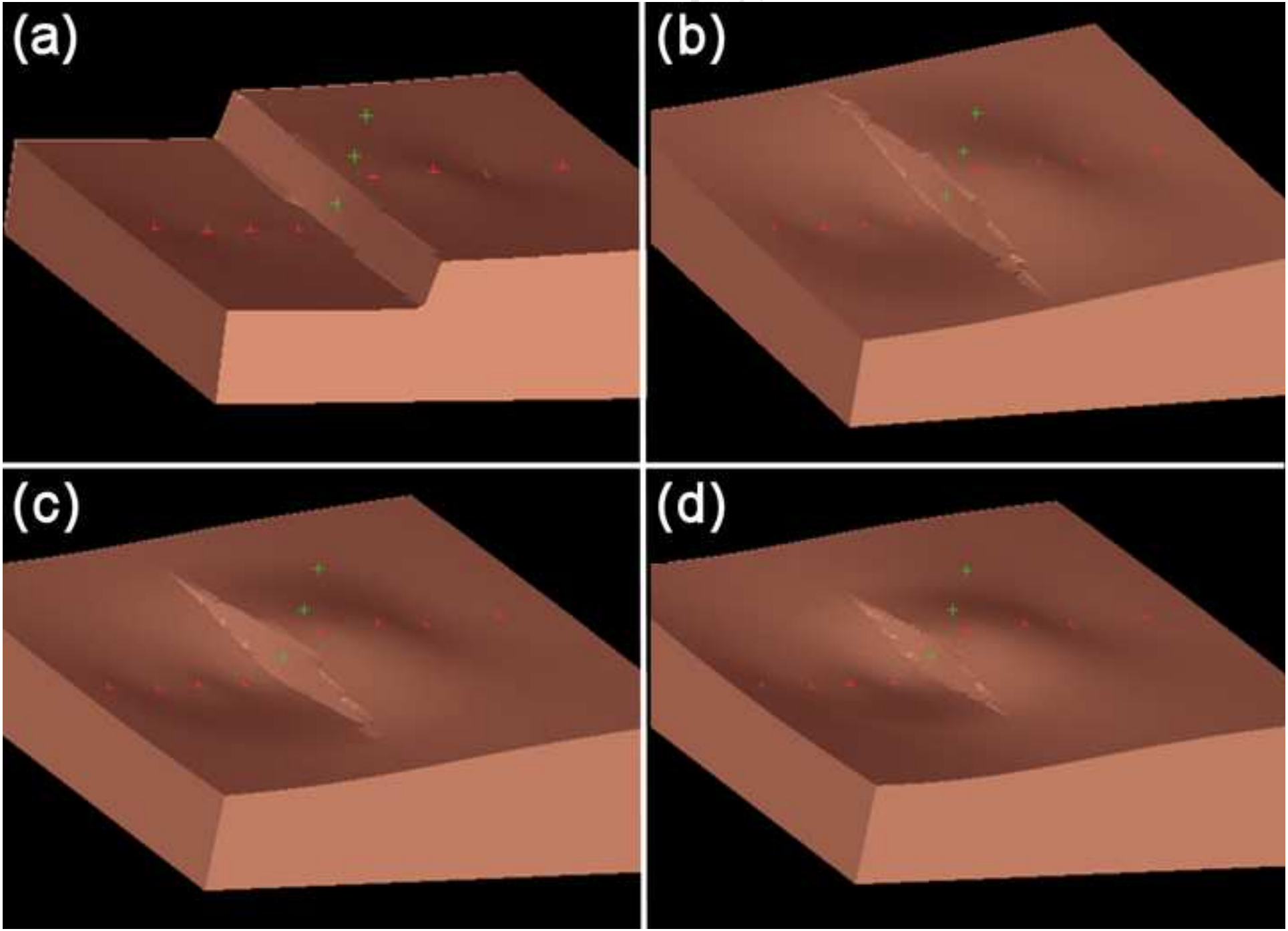

Figure6

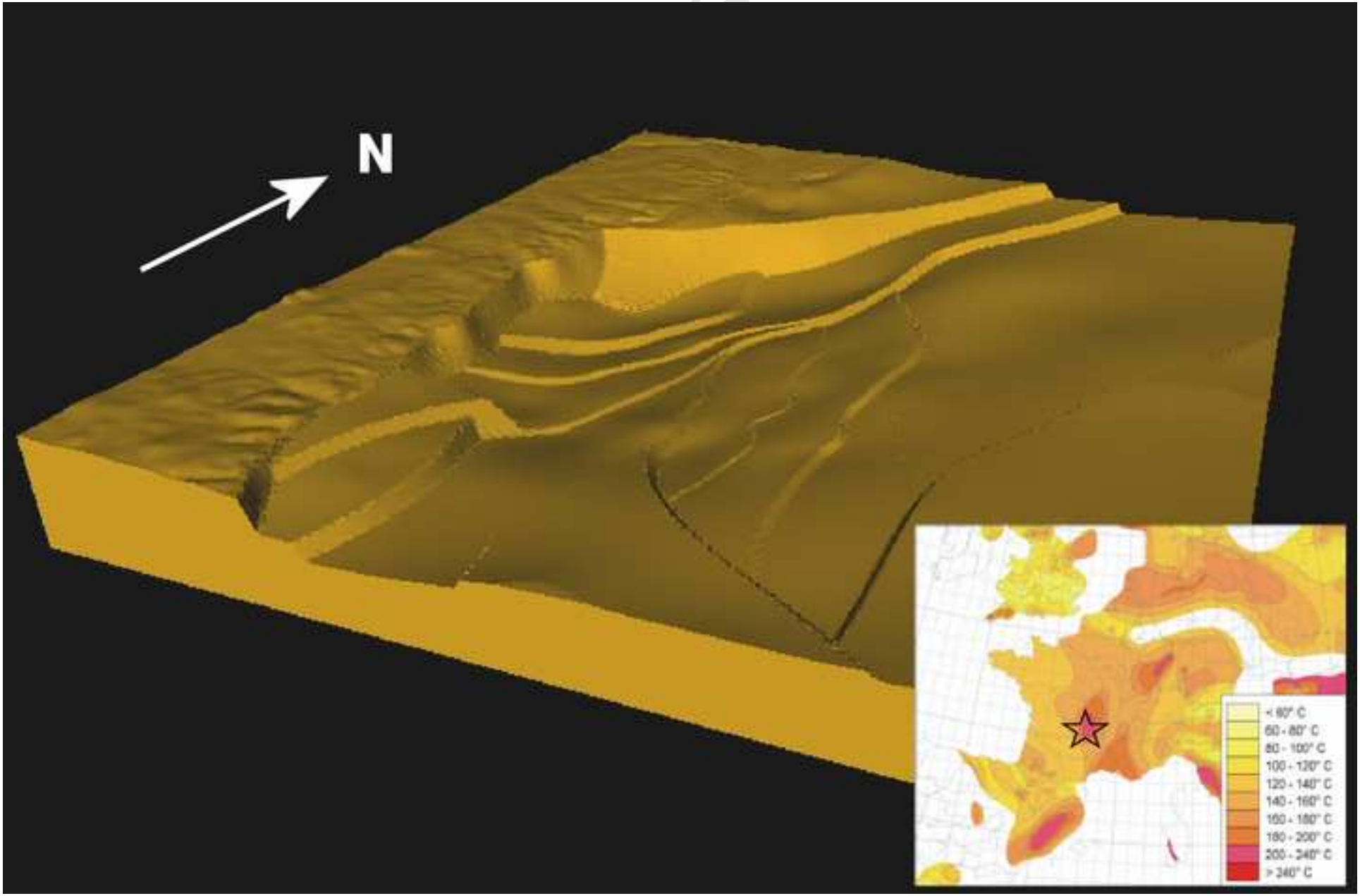
N
< 60° C
60 - 80° C
80 - 100° C
100 - 120° C
120 - 140° C
140 - 160° C
160 - 180° C
180 - 200° C
200 - 240° C
> 240° C

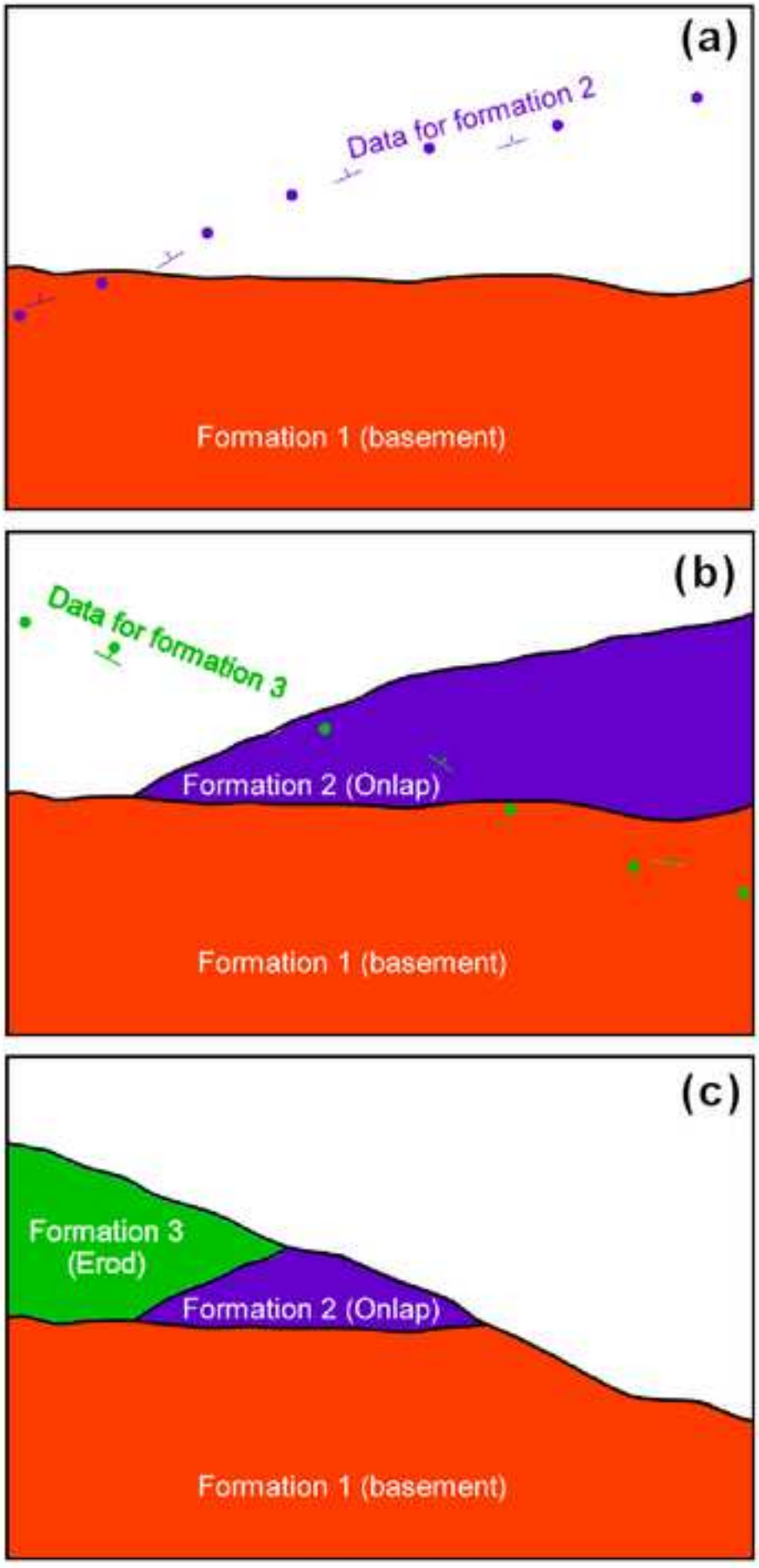

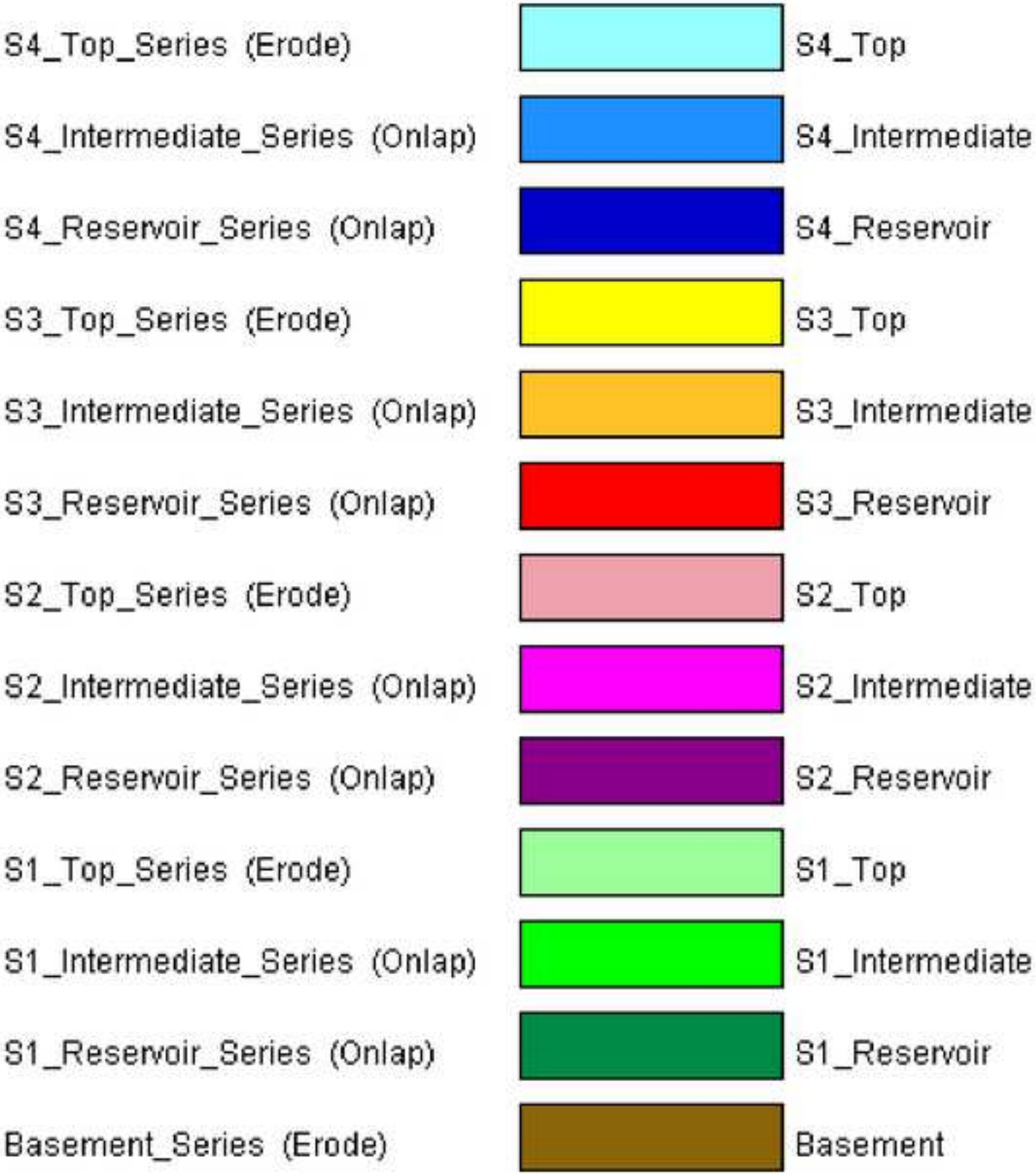

Figure9